

# Index-Modulated Circularly-Shifted Chirps for Dual-Function Radar & Communication Systems

Safi Shams Muhtasimul Hoque\*, Alphan Şahin\*

\*Electrical Engineering Department, University of South Carolina, Columbia, SC, USA

Email: shoque@email.sc.edu, asahin@mailbox.sc.edu

**Abstract**—In this study, we analyze index modulation (IM) based on circularly-shifted chirps (CSCs) for dual-function radar & communication (DFRC) systems. We develop a maximum likelihood (ML) range estimator that considers multiple scatters. To improve the correlation properties of the transmitted waveform and estimation accuracy, we propose index separation (IS) which separates the CSCs apart in time. We theoretically show that the separation can be large under certain conditions without losing the spectral efficiency (SE). Our numerical results show that the IS combined ML and linear minimum mean square error (LMMSE)-based estimators can provide approximately 3 dB signal-to-noise ratio (SNR) gain in some cases while improving estimation accuracy substantially without causing any bit-error ratio (BER) degradation at the communication receiver.

**Index Terms**—Chirps, DFRC, DFT-spread OFDM, PMEPR

## I. INTRODUCTION

The convergence of communication and radar functionalities within one wireless system addresses the under-utilized radar spectrum and the co-existence between radars and communication networks [1]. It also offers a new framework for wireless sensing applications such as gesture recognition and behavior prediction [2], [3]. On the other hand, it causes a trade-off between communications and radar as the resources may need to be shared between two applications. One way to circumvent this issue is to exploit communication signals for radar. However, the communication signals can deteriorate the accuracy of the estimation algorithms since their time and frequency characteristics are functions of the information bits [1]. In this study, we address this issue through circularly-shifted chirps (CSCs) and index modulation (IM).

In the literature, various techniques have been investigated to successfully employ communication signals for radar applications. For example, in [4], orthogonal frequency division multiplexing (OFDM) is considered for simultaneous radar and communications, and several range profiles are demonstrated. In [5] and [6], maximum likelihood (ML)-based range and velocity estimators for a single target are developed to achieve a finer resolution with OFDM-based radar with arbitrary phase-shift keying (PSK)-symbols and its implementation aspects are discussed. In [7], a generalized multicarrier model is investigated for radar, and time/frequency diversity techniques are evaluated. The issue of high peak-to-mean envelope power ratio (PMEPR) of multicarrier waveforms is also mentioned. An iterative algorithm based on filtering and clipping [8] is investigated in [9] to reduce the PMEPR at a cost of the distorted correlation function of the transmitted

waveform. In [10], arbitrary sequences are sent through the unused subcarriers in an OFDM system for radar functionality. In [11], the coexistence of frequency-modulated continuous-wave (FMCW) radars and communication systems are analyzed and a distributed networking protocol for interference mitigation is proposed. In [12], FMCW and OFDM waveform are transmitted simultaneously (i.e., transmit power is shared) and the fixed FMCW is utilized as a reference symbol to estimate velocity and range. IM, originally proposed in [13] for energy-efficient communications, has been considered and extended to multiple antennas in several works, e.g., [14]–[16] for dual-function radar & communication (DFRC) applications. In [15] and [16], IM is utilized with a multi-input multi-output (MIMO) radar by selecting a subset of subcarriers and/or transmit antennas. In [16], a minimal degradation at the radar receiver (RXr) with IM is emphasized by comparing it with OFDM. In [17], complementary sequences (CSs) in IEEE 802.11ad single carrier preamble are utilized for wireless sensing. To the best of our knowledge, CSCs with IM have not been investigated rigorously for DFRC in the literature.

In this study, we consider the scheme proposed in [18], which limits the PMEPR theoretically and allows to one generate arbitrary CSCs by introducing a special frequency-domain spectral shaping (FDSS) to discrete Fourier transform-spread orthogonal frequency division multiplexing (DFT-s-OFDM) adopted in 3GPP Fifth Generation (5G) New Radio (NR) [19]. We first develop an ML range estimator that considers multiple targets. We then discuss how to remove the impact of the waveform for accurate range estimation. To eliminate the spikes due to the multiple-chirp transmission within the estimation range, we propose index separation (IS) that ensures that the chirps are well-separated in time. We theoretically obtain the limit of separation that does not reduce the spectral efficiency (SE). We show that IS not only improves the estimation accuracy but also improves the performance at the communication receiver (RXc) through numerical analyses.

The rest of the paper is organized as follows. In Section II, we outline our system model. In Section III, we discuss estimation algorithms and the IS. In Section IV, we provide our numerical results. We conclude the paper in Section V.

*Notation:* The sets of complex numbers, real numbers, and positive integers are denoted by  $\mathbb{C}$ ,  $\mathbb{R}$ , and  $\mathbb{Z}^+$ , respectively. Complex conjugation is denoted by  $(\cdot)^*$ . The constants  $j$  and  $e$  denote  $\sqrt{-1}$  and Euler number, respectively.

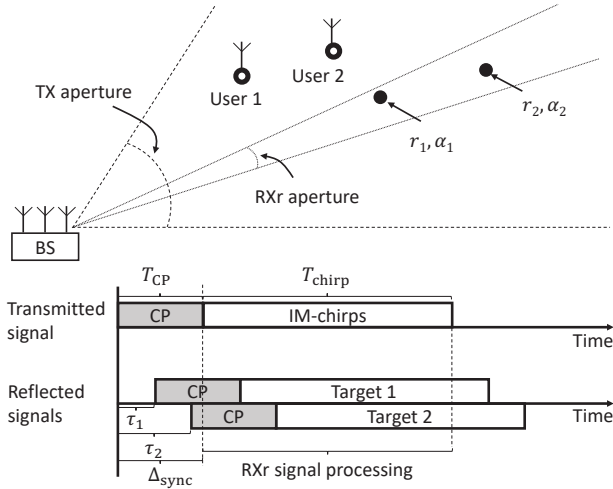


Figure 1. DFRC scenario and the corresponding timing diagram for the transmitted signal and the radar return for two targets.

## II. SYSTEM MODEL

### A. Scenario

Consider a DFRC scenario where a base station (BS) broadcasts  $p$  information bits to users while utilizing the same signal for radar functionality as illustrated in Figure 1. To resolve the angle information of the reflected paths while broadcasting information, we assume that the BS utilizes a wider antenna aperture  $\theta_{TX}$  at the transmitter (TX) as compared to the RXr antenna aperture  $\theta_{RX}$  and sweeps the RXr beam to different directions [20]. In this study, we assume that the BS operates in full-duplex mode [21] and the TX and RXr at the BS are synchronized in time, i.e., the RXr knows when the TX starts transmission.

Let  $\alpha_i \in \mathbb{R}$  and  $r_i \in \mathbb{R}$  be the path gain of the path TX-to- $i$ th target-to-RXr and the distance between the  $i$ th target and BS, respectively. By assuming a low-velocity environment (e.g., an indoor environment) as compared to the duration of the transmitted waveforms, we express the time-invariant impulse response of the channel as

$$h(\tau) = \sum_{i=1}^R \alpha_i \delta(\tau - \tau_i), \quad (1)$$

where  $\tau_i = 2r_i/c$  and  $\tau_i \leq \tau_{i+1}$ ,  $R$  is the number of reflections, and  $c$  is the speed of light. Our goal is to estimate  $\{r_i\}$  while using the same signal for broadcasting information. We assume that the maximum number of detectable targets is known at the receiver.

### B. Modulation and Waveform

In this study, we utilize the scheme proposed in [18] as DFRC waveform. In this scheme,  $p$  information bits are first grouped into two parts:  $p_1$  selector bits to choose  $L$  distinct chirps from a set  $\mathbb{W} = \{B_m(t) | m = 0, 1, \dots, M-1\}$  and  $p_2$  bits for  $L$  different  $H$ -PSK symbols. Let  $\mathcal{I} = \{i_0, i_1, \dots, i_{L-1}\}$  and  $\mathcal{S} = \{s_0, s_1, \dots, s_{L-1}\}$  be the sets of indices of selected

chirps and the corresponding  $H$ -PSK symbols, respectively. The complex baseband signal  $p(t)$  can then be expressed as

$$p(t) = \frac{1}{\sqrt{L}} \sum_{\ell=0}^{L-1} s_\ell B_{i_\ell}(t), \quad (2)$$

where  $B_m(t) = e^{j\psi_m(t)}$  is the  $m$ th circular translation of an arbitrary band-limited function with the duration  $T_{\text{chirp}}$ , where  $\tau_m = m/M \times T_{\text{chirp}}$  is the amount of circular shift for  $m = \{0, 1, \dots, M-1\}$  and the maximum frequency deviation of  $B_m(t)$  around the carrier frequency is  $D/2T_{\text{chirp}}$ . Since  $L$  indices can be chosen from  $M$  indices in  $\binom{M}{L}$  ways and  $L$   $H$ -PSK symbols are utilized, the scheme allows  $p = p_1 + p_2$  information bits to be transmitted, where  $p_1 = \lfloor \log_2 \left( \binom{M}{L} \right) \rfloor$  and  $p_2 = L \log_2(H)$ .

By using Fourier series, we can approximately express  $B_m(t)$  as

$$B_m(t) \approx \sum_{k=L_d}^{L_u} c_k e^{j2\pi k \frac{t-\tau_m}{T_{\text{chirp}}}}, \quad (3)$$

where  $L_d < 0$  and  $L_u > 0$ , and  $c_k$  is the  $k$ th Fourier coefficient of  $B_0(t)$ . The approximation in (3) is accurate for  $L_d < -D/2$  and  $L_u > D/2$  since  $B_{\tau_m}(t)$  is a band-limited function. By sampling  $p(t)$  with the period of  $T_{\text{sample}} = 1/f_{\text{sample}} = T_{\text{chirp}}/N$ , (2) can be approximately expressed in discrete time as [19]

$$p[n] = \frac{1}{\sqrt{L}} \sum_{k=L_d}^{L_u} c_k \underbrace{\sum_{m=0}^{M-1} d_m e^{-j2\pi k \frac{m}{M}}}_{\text{M-point DFT}} e^{j2\pi k \frac{n}{N}}, \quad (4)$$

Frequency-domain spectral shaping  
N-point IDFT with zero-padding

where  $d_{i_\ell} = s_\ell$ ,  $d_{i \notin \mathcal{I}} = 0$ , and  $N > M = L_u - L_d + 1 > D$ . Therefore, (2) can be implemented with a DFT-s-OFDM transmitter with an FDSS that leads to chirps and demodulated with a typical DFT-s-OFDM receiver as shown in Figure 2. To facilitate the equalization at the RXc, we prepend a cyclic prefix (CP) to the symbol with the duration of  $T_{CP} = N_{CP}T_{\text{sample}}$ , where  $N_{CP}$  is the number of samples in the CP duration. Note that this scheme results in a signal where its PMEPR is always equal or less than  $10 \log_{10}(L)$  dB and leads to CSs for  $L = 2$  [18]. Also,  $c_k$  is given in closed-form by using Fresnel integrals and Bessel functions for linear and sinusoidal chirps in [19], respectively.

At the RXr, we assume  $\tau_R \leq T_{CP}$  and an ideal phase/frequency synchronization between the TX and RXr carriers (e.g., fed through the same oscillator). After removing the CP and applying discrete Fourier transform (DFT), the received signal can be expressed as

$$b_k = H_k c_k \sum_{m=0}^{M-1} d_m e^{-j2\pi k \frac{m}{M}} e^{j2\pi k \frac{n}{N}} + \eta_n, \quad (5)$$

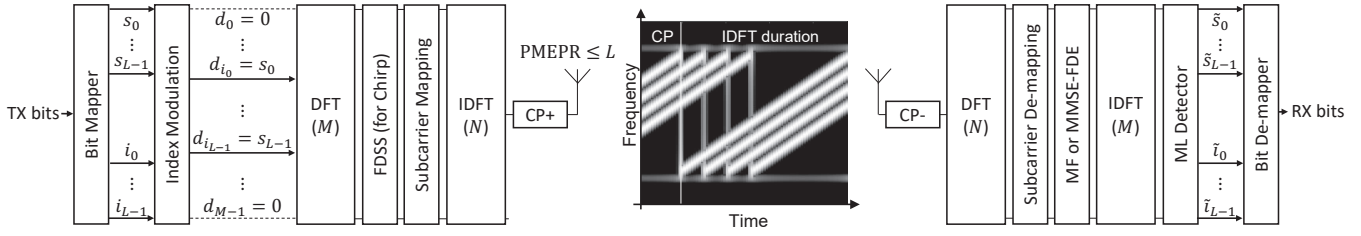


Figure 2. Transmitter and receiver block diagrams, and an signal synthesized with the transmitter for  $L = 4$  chirps.

where  $\eta_n$  is zero-mean additive white Gaussian noise (AWGN) with the variance of  $\sigma_n^2$  and  $H_k$  is the channel frequency response (CFR) given by

$$H_k = \int h(\tau) e^{-j2\pi f\tau} d\tau \Big|_{f=f_c + \frac{k}{T_{\text{chirp}}}} \quad (6)$$

$$= \sum_{i=1}^R \alpha_i e^{-j2\pi f_c \tau_i} e^{-j2\pi k \frac{\tau_i}{T_{\text{chirp}}}}, \quad (7)$$

Based on our system model, the maximum range is equal to  $c \times T_{\text{CP}}/2$  meters.

### III. RANGE ESTIMATION WITH INDEX-MODULATED CSCS

The received symbols in (5) can be re-expressed as

$$\mathbf{b} = \underbrace{\text{diag}\{\mathbf{c}\}}_{\mathbf{W} \triangleq \text{diag}\{\mathbf{w}\}} \text{diag}\{\mathbf{D}_M \mathbf{d}\} \mathbf{h} + \mathbf{n}, \quad (8)$$

where  $\mathbf{b}^T = [b_{L_d}, \dots, b_{L_u}]$ ,  $\mathbf{c}^T = [c_{L_d}, \dots, c_{L_u}]$ ,  $\mathbf{D}_M$  is the  $M$ -point DFT matrix,  $\mathbf{d}^T = [d_{L_d}, \dots, d_{L_u}]$ ,  $\mathbf{n}^T = [\eta_{L_d}, \eta_{L_d+1}, \dots, \eta_{L_u}]$ ,  $\mathbf{w}^T = [w_{L_d}, \dots, w_{L_u}]$  is the response of the waveform in the frequency, and  $\mathbf{h}^T = [H_{L_d}, \dots, H_{L_u}]$  which can be expressed as

$$\mathbf{h} = \mathbf{T} \mathbf{a}, \quad (9)$$

where  $\mathbf{T} = [\mathbf{t}_{\tau_1} \ \mathbf{t}_{\tau_2} \ \dots \ \mathbf{t}_{\tau_R}] \in \mathbb{C}^{M \times R}$  is the delay matrix and  $\mathbf{t}_{\tau_i} = e^{-j2\pi f_c \tau_i} \times [e^{-j2\pi L_d \frac{\tau_i}{T_{\text{chirp}}}, \dots, e^{-j2\pi L_u \frac{\tau_i}{T_{\text{chirp}}}}]$ , and  $\mathbf{a} = [\alpha_1, \alpha_2, \dots, \alpha_R]$ . For our DFRC scenario, the sets  $\mathcal{S}$  and  $\mathcal{I}$  are available at the RXr. Therefore, the symbols on the subcarriers, i.e.,  $\mathbf{w}$ , can be used as reference symbols. Hence, in AWGN channel, the ML-based delay estimation problem can be expressed as

$$\begin{aligned} \{\tilde{\tau}_i, \tilde{\alpha}_i\} &= \arg \min_{\substack{\{\tilde{\tau}_i, \tilde{\alpha}_i\} \\ i=1, \dots, R}} \|\mathbf{b} - \mathbf{W} \mathbf{T} \hat{\mathbf{a}}\|_2^2 \\ &= \arg \min_{\substack{\{\tilde{\tau}_i, \tilde{\alpha}_i\} \\ i=1, \dots, R}} \|\mathbf{W} \mathbf{T} \hat{\mathbf{a}}\|_2^2 - 2\Re\{\hat{\mathbf{a}}^H \mathbf{T}^H \mathbf{W}^H \mathbf{b}\}. \end{aligned} \quad (10)$$

For a single target, (10) can be reduced to

$$\tilde{\tau}_1 = \arg \max_{\tilde{\tau}_1} |\Re\{\mathbf{t}_{\tau_1}^H \mathbf{W}^H \mathbf{b}\}|, \quad (11)$$

where  $\tilde{\alpha}_1 = \Re\{\mathbf{t}_{\tau_1}^H \mathbf{W}^H \mathbf{b}\} / (\mathbf{w}^H \mathbf{w})$  by equating the derivative of cost function with respect to  $\tilde{\tau}_1$  and  $\tilde{\alpha}_1$  to zeros. The absolute value in (11) is due to the fact that  $\alpha_1$  can be negative or positive. The solution of (11) corresponds to the optimum

matched filter (MF) and the objective function can be evaluated via a computer search. Note that  $\mathbf{t}_{\tilde{\tau}_i}$  is a function of the carrier frequency. Thus, the search should consider narrow enough steps to obtain the maximum. In this study, we utilize a refinement procure that increases the number of points around the coarse estimate point.

The solution of (10) is not trivial for  $R > 1$ . Therefore, we utilize (11) and consider an iterative procedure by subtracting the information related to  $(n-1)$ th target from the signal as

$$\mathbf{b}^{(n)} = \mathbf{b}^{(n-1)} - \tilde{\alpha}_{n-1} \mathbf{W} \mathbf{t}_{\tilde{\tau}_{n-1}}, \quad (12)$$

where  $\mathbf{b}^{(1)} = \mathbf{b}$ . After  $\tilde{\tau}_i$  is estimated, the corresponding range can be obtained as  $\tilde{r}_i = \tilde{\tau}_i \times c/2$ .

The reward function in (11) is a function of the waveform. Since we transmit multiple CSCs in our scheme, additional spikes occur in the auto-correlation function of the waveform depending on the indices of selected chirps. Hence, the reward function in (11) can be high at different values of  $\tilde{\tau}_1$  for  $L > 1$  although there is a single target. On the other hand, the successful cancellation of the  $(n-1)$ th reflected signal in (12) relies on the accurate estimate of the reflection coefficient. Where there are multiple targets, this issue can cause an inaccurate estimation of the reflection coefficient. In addition, remaining spikes under inaccurate cancellation can also degrade the accuracy of the delay estimation for the next target. To address this problem, we investigate two solutions: the IS unique to the investigated scheme and the utilization of the linear minimum mean square error (LMMSE)-based channel estimate for the range estimation.

#### A. Solution 1: Index Separation

The IS mitigates the impact of waveform on the range estimation by constraining the scheme in [18] such that CSCs are sufficiently separated apart in time. Let  $\mathcal{D}(i_i, i_j) \triangleq \min(|i_i - i_j|, M - |i_i - i_j|)$  be the distance between two indices. As discussed in Section II, the maximum detection range depends on  $N_{\text{CP}}$ . Therefore, if  $\mathcal{D}(i_i, i_j) > N_{\text{CP}} \times M/N$  holds true for any combination, no spike due to the simultaneous transmission of chirps occurs within the duration of CP.

Let  $\mathcal{C}$  denote the cardinality of the set consisting of all index combinations where  $\mathcal{D}(i_i, i_j) \geq S$  for  $i, j \in 1, 2, \dots, L$  where  $S$  is the minimum distance between two selected indices.

**Theorem 1.** For  $L = 2$ ,  $\mathcal{C} = \binom{M}{2} - M(S-1)$ .

*Proof.*  $\mathcal{D}(i_i, i_j) \geq S$  implies that  $S \leq |i_i - i_j| \leq (M - S)$ . On the other hand, the number of  $\{i_i, i_j\}$  combinations

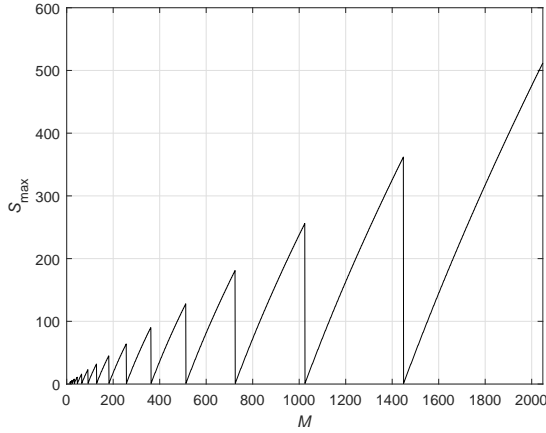


Figure 3.  $S_{\max}$  versus  $M$ . The distance between two indices can be as large as  $M/4$  without losing SE.

for  $|i_i - i_j| = a$  is  $M - a$ . Hence, the total number of  $\{i_i, i_j\}$  combinations for  $\mathcal{D}(i_i, i_j) \geq S$  is then equal to  $\mathcal{C} = \sum_{a=S}^{M-S} (M - a) = \binom{M}{2} - M(S - 1)$ .  $\square$

We do not have a closed-form solution of  $\mathcal{C}$  for  $L > 2$ . Note that the number of spikes in the auto-correlation function of the transmitter waveform and the PMEPR of  $p(t)$  increase with  $L$ . With this concern in mind, we limit our focus on  $L = \{2\}$  for the IS in this study.

For a given  $S$ , the SE of the investigated scheme can be calculated as  $\rho = \lfloor \log_2(\mathcal{C} \times H^L) \rfloor / M$ . Hence, one interesting question is that what is the largest  $S$  such that the SE still remains at the maximum for  $S = 1$  and  $L = 2$ ? Theorem 1 provides insight into the largest  $S$  as follows:

**Corollary 2.** Let  $\lfloor \log_2 \binom{M}{2} \rfloor = \lfloor \log_2 \mathcal{C} \rfloor$ . For  $L = 2$ ,  $S \leq S_{\max} \triangleq \lfloor 1 + \frac{\binom{M}{2} - 2^{\lfloor \log_2 \binom{M}{2} \rfloor}}{M} \rfloor$ .

*Proof.* If  $\lfloor \log_2 \binom{M}{2} \rfloor = \lfloor \log_2 \mathcal{C} \rfloor$ ,  $\log_2 \mathcal{C} \geq \lfloor \log_2 \binom{M}{2} \rfloor$  must hold. Hence,  $\mathcal{C} \geq 2^{\lfloor \log_2 \binom{M}{2} \rfloor}$ . By using Theorem 1, it can be written as

$$\mathcal{C} = \binom{M}{2} - M(S - 1) \geq 2^{\lfloor \log_2 \binom{M}{2} \rfloor}. \quad (13)$$

The inequality (13) can be rearranged as  $S \leq 1 + \frac{\binom{M}{2} - 2^{\lfloor \log_2 \binom{M}{2} \rfloor}}{M}$ , which implies that  $S \leq S_{\max}$ .  $\square$

In Figure 3, we plot  $S_{\max}$  for a given  $M$ . The surprising result is that the distance between indices can be as large as  $M/4$  without losing SE. For instance, for  $M = 2^k$ , where  $k \in \mathbb{Z}^+$ ,  $S_{\max}$  reaches its maximum value, i.e.,  $S_{\max} = M/4$ . On the other hand, we observe abrupt changes in  $S_{\max}$  for different values of  $M$ . For example,  $S_{\max}$  becomes minimum, i.e.,  $S_{\max} = 1$ , for  $M = 2^k + 1$ . This behavior is due to the fact that the number of bits that can be transmitted through the chirp indices increases by 1 if  $M = 2^k$  increases by 1. The IS guarantees a zone where the auto-correlation of the transmitted waveform is low, which improves the accuracy of

the reflection coefficient estimation. The duration of the zone can be equal to a typical CP size, e.g.,  $N/4$ , for certain values of  $M$  as  $S_{\max}/M = N_{\text{CP}}/N$  can be maintained.

The IS can also improve the RXr performance since it restricts the valid index combinations and reduce the interference between chirps when the MF is employed at the receiver. Assuming that FDSS is available at the RXr, the received symbols in the frequency are first multiplied with the conjugate of the composite response (i.e.,  $\{H_k^* c_k^*\}$ ). The inverse DFT (IDFT) of the processed vector is then calculated. Let  $(\tilde{d}_0, \tilde{d}_1, \dots, \tilde{d}_{M-1})$  be the modulation symbols after IDFT. The ML detector exploiting the IS for  $L = 2$  can be given by

$$\{\{\hat{m}, \hat{n}\}, \hat{s}_1, \hat{s}_2\} = \arg \max_{\substack{\{m,n\}, \hat{s}_1, \hat{s}_2 \\ \mathcal{D}(m,n) \geq S}} \Re \left\{ \tilde{d}_m \hat{s}_1^* + \tilde{d}_n \hat{s}_2^* \right\}, \quad (14)$$

where  $\mathcal{D}(m, n) \geq S$  reduces the search space. A low-complexity implementation of (14) can be done as follows: 1) Obtain  $\{i, k\}$  that maximizes  $\Re\{\tilde{d}_i e^{-j2\pi k/H}\}$  for  $i \in \{0, 1, \dots, M-1\}$  and  $k \in \{0, 1, \dots, H-1\}$  for the first index and the corresponding PSK symbol. 2) Evaluate the same function all other indices such that  $\mathcal{D}(i, n) \geq S$  for detecting the second index and the PSK symbol.

#### B. Solution 2: LMMSE-Based Channel Estimation

Another solution is to remove the impact of the waveform by using the LMMSE estimate of  $\mathbf{h}$ , i.e.,  $\hat{\mathbf{h}} = \mathbf{W}^H (\mathbf{W}\mathbf{W}^H + \sigma_n^2 \mathbf{I})^{-1} \mathbf{b}$  in the range estimation, rather than the vector  $\mathbf{W}^H \mathbf{b}$ . For a single target, the ML estimate of  $\tilde{\tau}_1$  can then be obtained as

$$\tilde{\tau}_1 = \arg \max_{\tilde{\tau}_1} |\Re\{t_{\tilde{\tau}_1}^H \mathbf{W}^H (\mathbf{W}\mathbf{W}^H + \sigma_n^2 \mathbf{I})^{-1} \mathbf{b}\}|, \quad (15)$$

where  $\tilde{\alpha}_1 = \Re\{t_{\tilde{\tau}_1}^H \mathbf{W}^H \mathbf{b}\} / (\mathbf{W}^H \mathbf{W} + \sigma_n^2 \mathbf{I})$ . For multiple targets, we also consider the iterative procedure in (12).

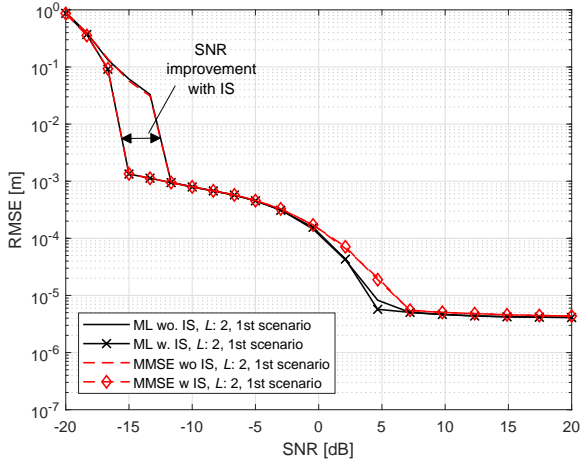
The main disadvantage of this method is the signal-to-noise ratio (SNR) degradation as compared to ML as demonstrated in the numerical results in Section IV. This solution has no impact on DFRC waveform design. On the other hand, it can also be utilized with IS to improve the estimation accuracy.

## IV. NUMERICAL RESULTS

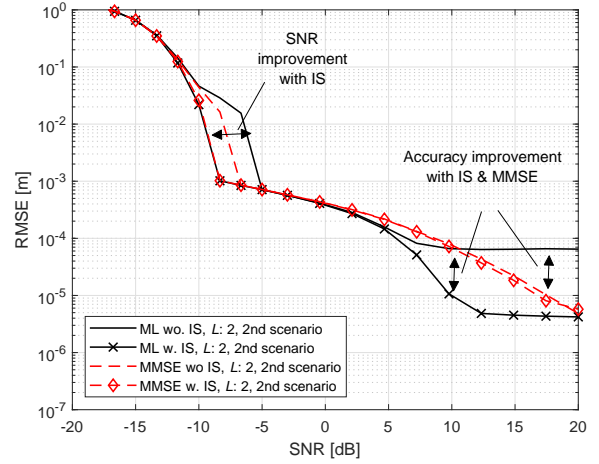
In this section, we consider IEEE 802.11ay OFDM mode with 4 channels, where the center frequency is  $f_c = 64.8$  GHz,  $f_{\text{sample}} = 10.56$  Gsps,  $N = 2048$ ,  $N_{\text{CP}} = 512$ , which lead to  $T_{\text{chirp}} \approx 194$  ns and  $T_{\text{CP}} \approx 48.48$  ns. We assume that  $M = 1448$ ,  $L_u = 724$ ,  $L_d = -723$ , and  $D = 1300$ . Therefore, the bandwidth of the signal is approximately 6.7 GHz and  $S_{\max}$  is equal to 362. The maximum range of the radar is 7.27 m. We set  $H = 2$ . Therefore,  $p = 11, 21$ , and 41 information bits are transmitted for  $L = 1, 2$ , and 4 chirps, respectively.

#### A. Radar Performance

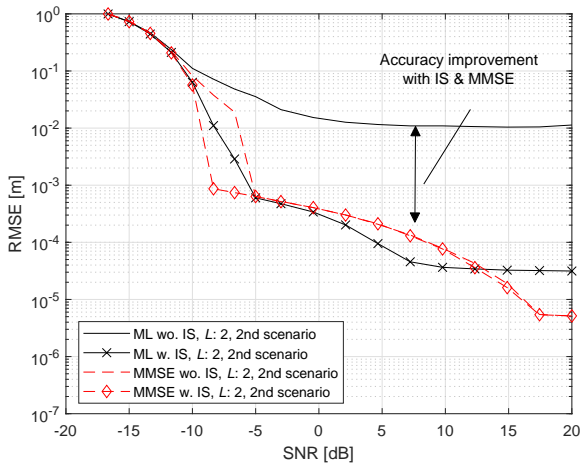
We consider two scenarios for evaluating RXr performance. In the first scenario, a single target is assumed. Its location is drawn from a uniform distribution between 0.5 m and 6.5 m and the reflection coefficient is set to  $-1$  considering the phase



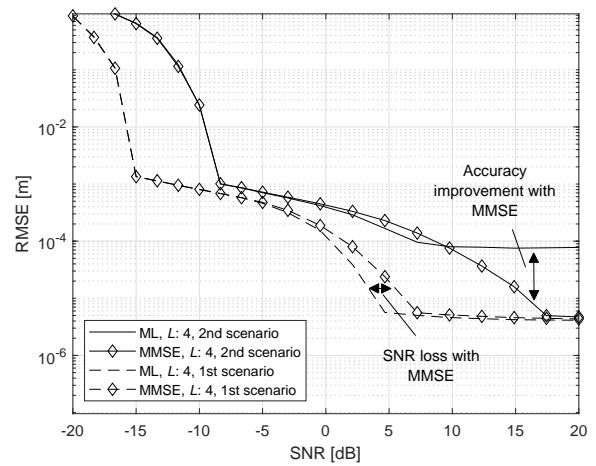
(a) Linear chirps, Scenario 1,  $L = 2$ .



(b) Linear chirps, Scenario 2,  $L = 2$ .



(c) Sinusoidal chirps, Scenario 2,  $L = 2$ .



(d) Linear chirps, Scenario 2,  $L = 4$ .

Figure 4. Impact of IS and MMSE on the RMSE versus SNR curves for different cases with CSCs.

change for the reflected signal [22]. For the second scenario, we consider two targets. While the first target is located at between 1.3 m and 3.3 m with the reflection coefficient of -1, the second target is between 3.6 m and 5.6 m with the reflection coefficient of -0.5.

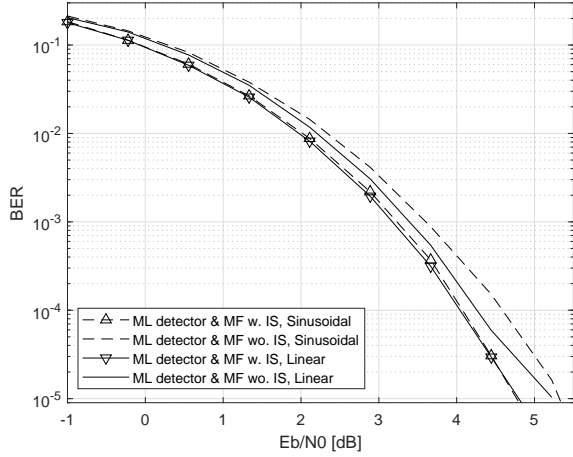
In Figure 4, we provide the root-mean-square error (RMSE) versus SNR curves with linear and sinusoidal chirps for  $L = \{2, 4\}$ . In Figure 4(a)-4(c), we observe substantial improvements in both SNR and/or accuracy when ML estimation is combined with IS. Since the IS eliminates the combinations where two indices are closed to each other, it avoids the spikes due to the waveform within the desired range. For Scenario 1, as shown in Figure 4(a), it provides approximately 3 dB SNR gain at low SNRs. Since there is only one target in this scenario, the cancellation in (12) does not occur. Therefore, there is no difference in terms of accuracy at high SNR among the methods. IS also provides SNR gain when it is utilized with LMMSE-based method. For Scenario 2, as in Figure 4(b), the IS improves the accuracy as the reflection coefficients are estimated more accurately. LMMSE also improves the accuracy at

the expense of a large SNR loss. In Figure 4(c), we repeat the simulation for sinusoidal chirps. Without removing the impact of the waveform, the RMSE increases dramatically. However, the accuracy improves with LMMSE-based estimation or IS. In Figure 4(d), we analyze the impact of  $L = 4$  chirps on RMSE without IS. LMMSE-based estimation is superior to the one with ML in terms of accuracy for Scenario 2 while it causes 2-3 dB SNR loss for Scenario 1.

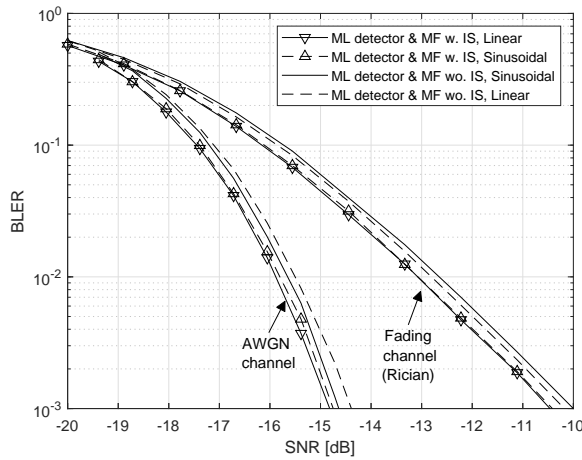
## B. Communication Performance

In Figure 5, the impact of IS on error-rate is analyzed for linear and sinusoidal chirps under AWGN channel and fading channel (i.e., three paths where the power delay profile is 0 dB, -10 dB, -20 dB at 0 ns, 10 ns, and 20 ns with Rician factors of 10, 0, and 0, respectively). In both configurations, block-error rate (BLER) and bit-error ratio (BER) improve slightly (i.e., 0.3 dB) when IS is employed.

We also measurement maximum PMEPR for linear and sinusoidal chirps for  $L = \{1, 2, 4\}$ . While the maximum PMEPRs are 2.7, 4.6, and 6.6 dB for linear chirps, they are 0,



(a) BER comparison.



(b) BLER comparison.

Figure 5. RXc performance with and without the IS.

3 and 6 dB for sinusoidal chirps for  $L = \{1, 2, 4\}$ , respectively. The reason why linear chirp diverges from the theoretical limit is the heavy truncation of FDSS in the frequency domain [18].

## V. CONCLUSION

In this study, we analyze CSCs for DFRC systems and develop various range estimators for multiple targets. As the main contribution, we propose IS which separates the CSCs apart in time. We theoretically obtain the maximum separation for  $L = 2$  without sacrificing SE. The limit indicates that the separation can be large under certain conditions. With numerical results, we show that the IS combined ML and LMMSE can provide approximately 3 dB SNR gain while improving estimation accuracy substantially. Also, we demonstrate that IS can slightly improve the BER performance. As future work, the study will be extended by considering the mobility in the environment with a realistic reflection model and multiple TX and RXs into account through a bi-static radar configuration.

## REFERENCES

- [1] B. Paul, A. R. Chiriyath, and D. W. Bliss, "Survey of RF communications and sensing convergence research," *IEEE Access*, vol. 5, pp. 252–270, 2017.
- [2] C.-Y. Hsu, R. Hristov, G.-H. Lee, M. Zhao, and D. Katabi, "Enabling identification and behavioral sensing in homes using radio reflections," in *Proc. CHI Conference on Human Factors in Computing Systems*, ser. CHI'19, New York, NY, USA, 2019, pp. 1–13.
- [3] J. Lien, N. Gillian, M. E. Karagozler, P. Amihoud, C. Schwesig, E. Olson, H. Raja, and I. Poupayev, "Soli: Ubiquitous gesture sensing with millimeter wave radar," *ACM Trans. Graph.*, vol. 35, no. 4, Jul. 2016.
- [4] C. Sturm, T. Zwick, and W. Wiesbeck, "An OFDM system concept for joint radar and communications operations," in *IEEE Vehicular Technology Conference (VTC)*, 2009, pp. 1–5.
- [5] M. Braun, C. Sturm, and F. K. Jondral, "Maximum likelihood speed and distance estimation for OFDM radar," in *IEEE Radar Conference (RadarConf)*, 2010, pp. 256–261.
- [6] M. Bičá and V. Koivunen, "Delay estimation method for coexisting radar and wireless communication systems," in *IEEE Radar Conference (RadarConf)*, 2017, pp. 1557–1561.
- [7] —, "Generalized multicarrier radar: Models and performance," *IEEE Trans. Signal Process.*, vol. 64, no. 17, pp. 4389–4402, Sep. 2016.
- [8] P. Stoica, H. He, and J. Li, "New algorithms for designing unimodular sequences with good correlation properties," *IEEE Transactions on Signal Processing*, vol. 57, no. 4, pp. 1415–1425, Jan. 2009.
- [9] S. Sharma, M. Bičá, and V. Koivunen, "Reduced PMEPR multicarrier radar waveform design," in *IEEE Asilomar Conference on Signals, Systems, and Computers*, 2019, pp. 2048–2052.
- [10] S. D. Liyanaarachchi, C. B. Barneto, T. Riihonen, and M. Valkama, "Joint OFDM waveform design for communications and sensing convergence," in *Proc. IEEE International Conference on Communications (ICC)*, 2020, pp. 1–6.
- [11] C. Aydogdu, M. F. Keskin, N. Garcia, H. Wymeersch, and D. W. Bliss, "RadChat: Spectrum sharing for automotive radar interference mitigation," *IEEE Trans. Intell. Transp. Syst.*, pp. 1–14, Dec. 2019.
- [12] M. M. Şahin and H. Arslan, "Multi-functional coexistence of radar-sensing and communication waveforms," *CoRR*, vol. abs/2007.05753, Jul. 2020.
- [13] E. Başar, Ü. Aygözü, E. Panayircı, and H. V. Poor, "Orthogonal frequency division multiplexing with index modulation," *IEEE Trans. Signal Process.*, vol. 61, no. 22, pp. 5536–5549, Aug. 2013.
- [14] E. BouDaher, A. Hassanien, E. Aboutanios, and M. G. Amin, "Towards a dual-function MIMO radar-communication system," in *Proc. IEEE Radar Conference (RadarConf)*, 2016, pp. 1–6.
- [15] D. Ma, T. Huang, N. Shlezinger, Y. Liu, X. Wang, , and Y. C. Eldar, "A DFRC system based on multi-carrier agile FMCW MIMO radar for vehicular applications," in *Proc. IEEE International Conference on Communications (ICC)*, 2020, pp. 1–6.
- [16] D. Ma, N. Shlezinger, T. Huang, Y. Liu, and Y. C. Eldar, "Joint radar-communication strategies for autonomous vehicles: Combining two key automotive technologies," *IEEE Signal Process. Mag.*, vol. 37, no. 4, pp. 85–97, Jun. 2020.
- [17] P. Kumari, J. Choi, N. González-Prelcic, and R. W. Heath, "IEEE 802.11ad-based radar: An approach to joint vehicular communication-radar system," *IEEE Trans. Veh. Technol.*, vol. 67, no. 4, pp. 3012–3027, Apr. 2018.
- [18] S. Hoque, C.-Y. Chen, and A. Şahin, "A wideband index modulation with chirp-based complementary sequences," in *Proc. IEEE Consumer Communications & Networking Conference (CCNC) (submitted)*, Jan. 2021, pp. 1–6.
- [19] A. Şahin, N. Hosseini, H. Jamal, and D. W. Matolak, "DFT-spread-OFDM based chirp transmission," *CoRR*, vol. abs/2008.03766, Aug. 2020.
- [20] J. Li and P. Stoica, "MIMO radar with colocated antennas," *IEEE Signal Process. Mag.*, vol. 24, no. 5, pp. 106–114, 2007.
- [21] P. Kumari, A. Mezghani, and R. Heath, "JCR70: A low-complexity millimeter-wave proof-of-concept platform for a fully-digital MIMO joint communication-radar," *CoRR*, vol. abs/2006.13344, Jun. 2020.
- [22] D. Tse and P. Viswanath, *Fundamentals of Wireless Communication*. Cambridge University Press, 2005.